GEOPHYSICAL RESEARCH LETTERS, VOL. 19, NO. 17, PAGES 1755-1758, SEPTEMBER 4, 1992

POLAR STRATOSPHERIC CLOUDS OVER MCMURDO, ANTARCTICA, DURING THE 1991 SPRING: LIDAR AND PARTICLE COUNTER MEASUREMENTS.

A. Adriani[1], T. Deshler[2], G.P. Gobbi[1], B.J. Johnson[2], G. Di Donfrancesco[3]

Abstract. Lidar and balloonborne particle counter measurements were performed simultaneously on two days when polar stratospheric clouds were observed in late August 1991 at McMurdo, Antarctica. Both nitric acid trihydrate and ice clouds were observed in the lower stratosphere between 10 and 23 km in different formation stages and with different cooling rate; however in all cases the size distributions were bimodal. Comparison of scattering ratios measured by lidar and calculated from particle size distributions are in good agreement; however, discrepancies were observed when the lower stratosphere was highly perturbed by wave activity. Lee waves generated by air flowing over the Trans Antarctic Mountains induced ice cloud formation at altitudes as high as 20 km. No PSCs were observed after the end of August in 1991.

Introduction

Polar stratospheric clouds (PSCs) are believed to play two essential roles in the ozone destruction process. They provide the surfaces necessary to permit chlorine (and bromine) to be released from reservoir species ($ClONO_2$ and HCl), and they sequester reactive nitrogen which would otherwise react with chlorine and thereby prevent it from destroying ozone [Solomon, 1990]. The very low temperatures of the Antarctic stratosphere and its dynamical stability during the winter and early spring provide the necessary conditions for the formation of PSCs, which are thought to be made by the condensation of nitric acid trihydrate $HNO_3 \cdot 3H_2O$ (NAT) and water on background aerosols [Crutzen and Arnold, 1986, Toon et al., 1986]. NAT begins condensing at least 5 K above the water frost point [Hanson and Mauersberger, 1988]. Further cooling may cause condensation of water. Due to the larger amount of H_2O with respect to HNO_3 (about 3 orders of magnitude in the stratosphere), ice cloud particles reach much larger sizes. Water ice clouds appear more rarely, and have characteristics closer to cirrus clouds.

During the 1991 spring combined measurements with lidar and balloon-borne particle counters were performed at McMurdo Station, Antarctica (78°S, 167°E). During springtime McMurdo is usually well inside the polar vortex and stratospheric temperatures can reach values low enough for the formation of PSCs. Although the ozone depletion observed over McMurdo, Antarctica, during spring 1991 was similar to the severe depletions observed in 1987, 1989 and 1990 [Johnson et al., 1992], in the period 26 August - 10 October, PSCs were detected over McMurdo only on 27 and 28 August. This paper describes these two events.

[1] Istituto di Fisica dell'Atmosfera, CNR, Frascati, Italy
[2] University of Wyoming, Laramie, WY, USA
[3] ENEA, AMB-MON/CRE Casaccia, Roma, Italy

Paper number 92GL01941
0094-8534/92/92GL-01941$03.00

Instruments

The lidar employed is based on a Nd-YAG laser emitting 140 mJ at 532 nm, a 41 cm Newtonian telescope with a field of view of 0.6 mrad, and a 0.15 nm bandwidth interference filter. Polarized and depolarized backscattered light are simultaneously detected. Maximum vertical resolution is 3 m, but is usually averaged to 150 m to improve the signal to noise ratio. The range of the system is approximately 26 km in the dark, and 20 km in daylight. A rotating shutter removes signal under 8 km to preserve the linearity of the detectors.

The primary information from lidars is the scattering ratio, R: the ratio of the total detected atmospheric echo to that expected from purely molecular scattering. Molecular backscattering is calculated from the atmospheric number density by means of temperature and pressure soundings. The lidar signal is calibrated by making it equal to the calculated molecular signal at an altitude where the atmosphere is assumed to be particle free. In Antarctica, calibration heights are usually chosen above 23 km, where the aerosol contribution to the scattering is commonly negligible [Gobbi et al., 1991], and the scattering ratio drops to minimum values. Particle counter measurements confirm the selection of the particle free region. The lidar also measures depolarization, D, which is reported here as the percentage of depolarized signal with respect to the total collected. When the optical depth of the cloud is sufficiently low, as in PSCs, contamination of the lidar echoes from multiple scattering is negligible and the depolarization is an indication of asphericity in the particle shape.

Balloonborne optical aerosol particle counters were used for "in situ" observations of aerosol number density for particles with radii $\geq$ 0.15, 0.25, 0.5, 1.0, 2.0, 3.0, 5.0 and 10.0 μm. Balloonborne aerosol counters have been used to study PSCs in Antarctica since 1987. Initial observations using the improved aerosol counters employed in these measurements were made in 1989 [Hofmann and Deshler, 1991]. Separate flights were also made using a similar aerosol counter with a vapor growth chamber on the inlet to measure the total aerosol population, or condensation nuclei (CN).

Between 26 August and 10 October the lidar collected 60 sets of measurements, while 12 balloonborne aerosol particle measurements were made, 5 for CN and 7 for optical aerosol. Different stratospheric conditions: background aerosol, PSCs, and volcanic clouds were sampled during this period.

Observations and Discussion

A summary of the occurrence of stratospheric clouds observed by lidar is depicted in Figure 1. At the end of August, temperatures reached values as low as 188 K at heights close to 20 km, and PSCs were detected. At the beginning of September, a displacement of the vortex boundary over the station induced a warming in the lower stratosphere above 193 K [Johnson et al.,1992]. This weakening of the polar vortex at the beginning of September permitted the entrainment of volcanic aerosols just above the tropopause level. The cloud, observed in the altitude range of 9 - 12 km, has been attributed to the Cerro Hudson eruption which occurred in Chile on 12-15 August [Deshler et al., 1992].

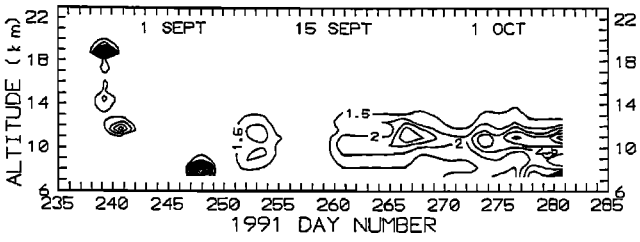

Figure 1. Time-height contours of lidar scattering ratio between 26 August and 10 October, 1991.

Simultaneous lidar and "in situ" measurements of PSCs were obtained on 27 and 28 August, Figures 2 and 3. The lidar profiles shown are averaged over 15 minutes, and each one corresponds approximately to the time when the aerosol counter was passing between 15 and 20 km. Both lidar and particle counters profiles are averaged for a 150 m resolution. On 5 September, an aerosol sounding in very clear conditions measured the stratospheric background aerosol which is reported in the figures as dashed lines. Particles with radii larger than 0.5 μm were absent in the background profile above 16 km.

The particle counter measurements were used to obtain lognormal size distributions to fit the particle size distributions in the PSCs. Concentrations of particle mass and surface area, and necessary vapor mixing ratios for HNO_3, assuming the particles are composed of NAT, are shown, along with the lognormal parameters, in Table 1. Bimodal distributions were primarily used. On 27 August at 13.8 km, and on 28 August at 17.1 and 18.9 km the computed HNO_3 vapor mixing ratios in the condensed phase are 2 to 3 times higher than the expected ambient concentrations at that time of the year. This suggests that the particles were mostly formed by ice. For the particles in these layers the computed H_2O vapor mixing ratios were a factor of 10 to 100 below the measured water mixing ratio of 2-3 ppmv.

The aerosol size distributions were also used to infer scattering ratios for different indices of refraction. In Table 1, these results

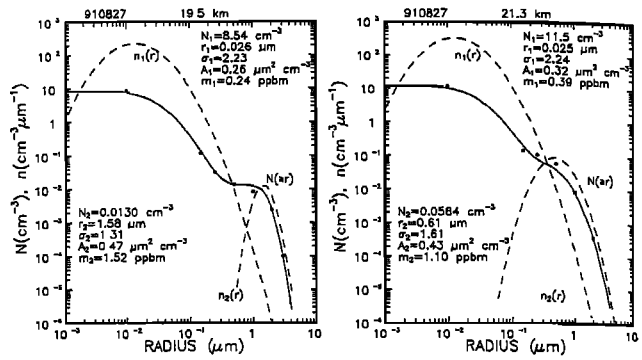

Figure 3. Particle size distributions from "in situ" aerosol measurements on 27 August at 19.5 and 21.3 km.

are compared with the measurements. Assuming the particles to be composed of NAT or 60% sulfuric acid solutions in water the appropriate indices are respectively 1.37 and 1.43; however, if the NAT particles have a crystalline rather than an amorphous structure, an index of refraction near 1.5 may be more appropriate [Toon et al., 1990]. Scattering ratio calculations assumed indices of refraction of 1.37 and 1.5. Observed depolarization is also reported in Table 1.

According to the "in situ" particle measurements on 27 August, Figure 2b, a broad region of the stratosphere was filled with a diffuse PSC. The concentration of particles with radius larger than 0.25 and 0.5 μm was increased above background values from 10 to 23 km, while for radius larger than 0.15 μm the increase above background did not occur until 18 km. Small features appear at 11, 14 km and thicker PSCs between 17.5 and 22 km. The broad diffuse region, the PSC layers, and the cirrus cloud, 5-7 km, were also all observed in the lidar profile, Figure 2a. The temperature was close to the condensation point for ice for 3 ppmv water vapor between 17 and 20 km and was below the condensation temperature for NAT for 2 ppmv H_2O and 1 ppbv

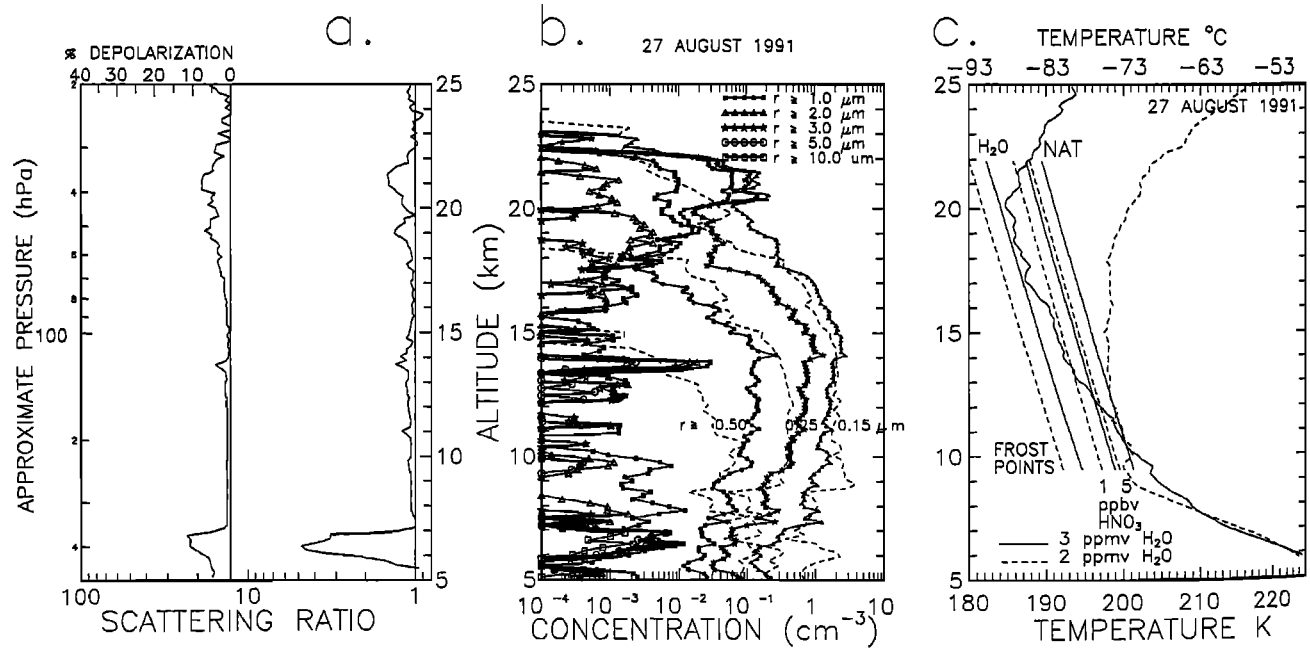

Figure 2. Lidar and particle counter measurements taken on 27 August: a) lidar depolarization (left side) and scattering ratio; b) aerosol particle concentration for 8 different radii, dashed curves are the background profiles from 5 September; c) temperature profiles, 27 August and 5 September (dashed). Water frost point and NAT condensation temperatures for 2, 3 ppmv H_2O and 1, 5 ppbv HNO_3 are also indicated.

TABLE 1. PSC Bimodal Lognormal Parameters: Number Density (N), Geometric Radius (r), Width (σ), Area, Mass, and Required HNO_3 Content. Lidar Computed and Measured Scattering Ratio (R), Lidar Percent Depolarization (D), and Air Parcel Cooling Rate

Press hPa	Alt km	Temp K	N_1 cm^{-3}	r_1 μm	σ_1	$Area_1$ $\mu m^2 cm^{-3}$	$Mass_1$ $\mu g\ m^{-3}$	HNO_3 ppbv	N_2 cm^{-3}	r_2 μm	σ_2	$Area_2$ $\mu m^2 cm^{-3}$	$Mass_2$ $\mu g\ m^{-3}$	HNO_3 ppbv	R(computed) (1.37)(1.50)	R	D	Cool.Rate K/Day
27 Aug.																		
115	13.8	193	13.9	0.064	2.30	2.88	0.380	0.67	0.022	3.37	1.38	3.87	5.64	10.9	1.58 1.79	1.32	3.9	5-7
112	14.0	193	13.1	0.107	1.76	3.55	0.280	0.55	0.001	3.21	1.31	0.16	0.21	0.41	1.09 1.21	1.23	0.5	-
57	17.7	188	7.63	0.052	1.81	0.51	0.021	0.08	0.002	2.98	1.27	0.31	0.35	1.33	1.09 1.10	1.11	2.8	1
45	19.1	186	6.94	0.052	1.69	0.40	0.014	0.07	0.019	1.44	1.52	0.71	0.53	2.52	1.24 1.29	1.33	6.8	1
41	19.5	186	8.11	0.028	2.17	0.26	0.011	0.06	0.013	1.21	1.75	0.46	0.41	2.10	1.16 1.20	1.16	5.4	-
30	21.3	186	11.5	0.025	2.24	0.32	0.013	0.10	0.058	0.62	1.58	0.43	0.15	1.08	1.17 1.35	1.46	7.3	10
28 Aug.																		
107	14.4	194	12.0	0.183	1.56	7.53	0.758	1.58	0.005	1.77	1.27	0.21	0.14	0.30	1.22 1.64	2.00	0.6	10-20
101	14.7	193	11.6	0.193	1.56	8.05	0.845	1.85	0.005	2.25	1.66	0.50	0.71	1.55	1.30 1.83	2.36	1.6	10-20
66	17.1	185	7.21	0.243	1.52	7.62	0.959	3.09	0.227	1.22	1.50	5.90	3.61	11.6	2.68 3.38	1.35	0.6	5
47	18.9	186	6.41	0.163	1.32	2.49	0.164	0.74	0.058	1.46	1.53	2.24	1.73	7.79	1.77 1.98	12.0	10.1	10
46	19.1	187	6.94	0.137	1.38	2.02	0.120	0.56	0.036	0.88	1.88	0.76	0.60	2.79	1.76 1.92	11.4	9.9	10

HNO_3 from 13 to 21.5 km. In the 1990 Antarctic spring the water vapor concentration in the lower stratosphere was found to be 2-3 ppmv [Hofmann et al., 1991]. Additional measurements, not yet published, in 1991 indicated the same range of values. Altough, the cloud at 14 km exhibits very sharp changes in size distribution between the top and bottom, the distribution in both layers is best represented with bimodal lognormal distributions (Table 1). The top of the layer is composed of mostly small particles. No lidar depolarization is observed and the first mode of the size distribution is the same as at the bottom. At the bottom, 150 m below, the second mode of the size distribution is significantly enhanced. The total number concentration, N_0, in the second mode is 20 times the value at the top. Particle sizes exceed 5 μm and are aspherical, the depolarization is about 4% and scattering ratio 1.3. The amount of HNO_3 necessary to make such particles (10 ppbv) is larger than the expected mixing ratio, suggesting that some ice must be present. This is consistent with a measured scattering ratio smaller than the computed one. The difference between the top and the bottom is consistent with gravitational settling of the larger particles.

Thicker PSC layers composed of aspherical particles were detected between 18 km and 22 km. The temperature was near the frost point for 3 ppmv water vapor between 17 and 20 km and particles larger than 3 μm radii were detected at 18-20 km while above 20 km particles only as large as 2 μ were observed . Even though more particles were contained in the layer at 21-22 km, larger particles in the layer at 19-19.5 km contained more mass (Table 1). Still the amount of vapor in the condensed phase is consistent with NAT rather than water. A comparison of the 27 August size distributions at 19.5 and 21.3 km is shown in Figure 3. Although the first mode of each distribution is similar, indicating condensation on the same background aerosol, the second mode is quite different. At 21.3 km the concentration of particles with $r \geq 0.15$, 0.25 and 0.5 μm are similar and the concentration of 0.25 and 0.5 μm radius particles are increased by a factor of 5 over their concentration at 19.5 km. Consequently at 21 km the large mode radius is decreased to less than half the value obtained at lower altitudes. Regions as this one, where condensation and growth occurs on most of the small particles, are typical of fast

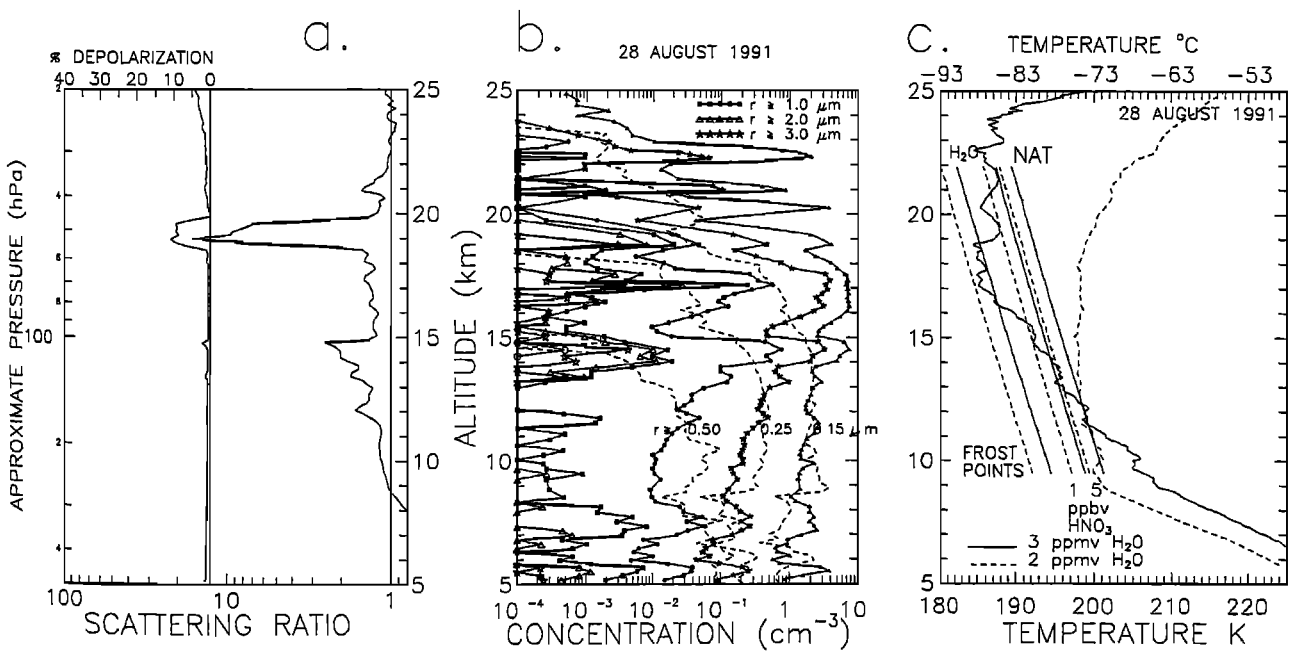

Figure 4. As in Figure 2, but for 28 August measurements.

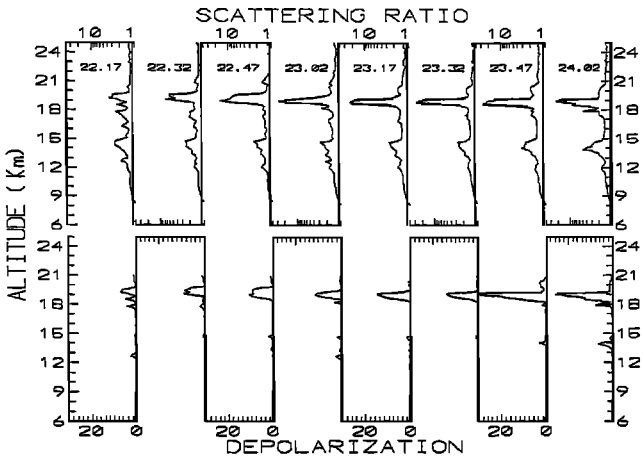

Figure 5. Polar Stratospheric Clouds on 28 August. Temporal evolution of lidar scattering ratio (a) and depolarization (b).

cooling whereas with slow cooling only a few of the larger particles grow [Hofmann et al., 1990]. These two size distributions illustrate this difference, and calculation of the cooling rate using isentropic back trajectory calculations [J. Harris, personal communication] confirm this, indicating a cooling rate of 1 K/day at 19.5 and 10 K/day at 21.3 km (Table 1).

The dynamical situation was quite different on 28 August when particle concentration were enhanced above background at altitudes above 12 km, Figure 4. Strong winds from the W-NW crossed the Trans Antarctic Mountains creating a lee wave structure in the air flow reaching Ross Island. Nacreous clouds were observed for many hours before the measurements. Evidence for this can be seen in the wave structure of the temperature profile and the particle counter profiles (Figure 4, b and c) in that region. Relative particle concentration maxima are observed corresponding to the temperature minima. Large discrepancies between the lidar and "in situ" measurements were observed in the upper levels indicating the small spatial scale of the cloud observed by lidar. At 19 km the sonde was 50 km from the lidar site. The particle counter profile shows a very thin layered structure in the region 18 - 23 km. Large particles were detected only in the lower layer around 19 km; however, the particle counter measurements between 19 and 22 km are sketchy due to data telemetry problems. In the layer at 19 km, lidar measurements reached scattering ratios up to 30 and depolarizations larger than 10%. This suggests an ice cloud consisting of aspherical ice crystals. The observed large scattering ratios require particle masses which can only be supplied by condensed water and the depolarization ratios suggest aspherical ice crystals. Figure 5 reports the scattering ratio and depolarization evolution during the two hours of measurement. The maximum scattering ratio (R=26) is reached at 23:32 with the maximum in depolarization (D= 30%) following in fifteen minutes. On the basis of Figure 5, the cloud lifetime was just a few hours. Lidar observations performed 8 hours later showed no evidence of this cloud. If the cloud formed in a lee wave, the downward displacement of the cloud barycentre of 150 m/hour, Figure 5, could be interpreted as the phase velocity of the wave perturbation.

Cooling rates [J. Harris, personal communication] are shown in Table 1 for the PSC layers examined. On 27 August, slower cooling rates permitted a few large particles to grow, while on the 28 August, with faster cooling rates, growth took place mainly on a larger number of particles in the first mode.

Conclusions

Between 26 August and 10 October, 60 sets of lidar measurements were collected and 12 balloonborne aerosol particle measurements were made, including condensation nuclei and optical aerosol. Two combined measurements were performed on PSCs at the end of August. In spite of severe ozone depletion these were the only two PSC sightings in this period. Bimodal lognormal distributions best represented the size distributions encountered in PSCs even during different formation stages. Agreement was found between calculated and measured scattering ratios primarily for indices of refractions near 1.5. This fact and the evidence of asphericity given by large depolarization values suggest that PSC particles condense in a crystalline structure even for relatively small sizes. The cooling rate strongly controls the number of particles on which NAT condensation occurs. Temperature fluctuations generated by lee waves in the troposphere were observed to propagate upward into the stratosphere and cause formation of ice clouds which had relatively short time and space scales.

Acknowledgments. The aerosol measurements were funded by the U.S. National Science Foundation, Division of Polar Programs. The lidar measurements were funded by the Italian National Program for Antarctic Research.

References

Crutzen P.J. and F. Arnold, Nitric acid cloud formation in the cold Antarctic stratosphere: a major cause for the springtime ozone hole, Nature, 324, 651-654, 1986

Gobbi G.P., T. Deshler, A. Adriani, and D.J. Hofmann: Evidence for denitrification in the 1990 Antarctic spring stratosphere: I lidar and Temperature measurements, Geophys. Res. Let., 18, 1995-1998, 1991.

Hanson, D and K. Mauersberger, Laboratory studies of the nitric acid trihydrate: Implication for the South Polar stratosphere, Geophys. Res. Let., 15, 855-858, 1988.

Hofmann D.J., T. Deshler, Stratospheric cloud observation during formation of the Antarctic ozone hole in 1989, J. Geophys. Res., 96D, 2897-2912, 1991.

Hofmann D.J., T. Deshler, F. Arnold, and H. Schlager, Balloon observations of nitric acid aerosol formation in the Arctic stratosphere: II. Aerosol, Geophys. Res. Let., 17, 1279-1282, 1990.

Hofmann D.J., S.J. Oltmans, and T. Deshler, Simultaneous balloonborne measurements of stratospheric water vapor and ozone in the polar regions, Geophys. Res. Let., 18, 1011-1014, 1991.

Johnson B.J., T. Deshler, R.L. Thompson, Vertical profiles of ozone at McMurdo Station, Antarctica: spring 1991, Geophys. Res. Let., in press, 1992.

Solomon S., Progress towards a quantitative understanding of Antarctic ozone depletion, Nature, 347, 347-354, 1990.

Toon O.B., E.V. Browell, S. Kinne, J. Jordan, An analysis of lidar observations of polar stratospheric clouds, Geophys. Res. Let., 17, 393-396, 1990.

Toon, O.B., P. Hamill, R.P. Turco, and J. Pinto, Condensation of HNO_3 and HCl in the winter polar stratosphere, Geophys. Res. Let., 13, 1284-1287, 1986.

A.Adriani and G.P.Gobbi, Istituto Fisica dell'Atmosfera, CNR, Frascati, Italia

T. Deshler and B.J. Johnson, University of Wyoming, Laramie, WY, USA

G. Di Donfrancesco, Ente Nazionale Energie Alternative AMB-MON/CRE Casaccia, Roma, Italia

(Received: June 18,1992
Accepted: July 31, 1992)